JTTEE5 20:100–107
DOI: 10.1007/s11666-010-9586-9
1059-9630/$19.00 © ASM International

Peer Reviewed

Mechanical Behavior of Air Plasma-Sprayed YSZ Functionally Graded Mullite Coatings Investigated via Instrumented Indentation

C.V. Cojocaru, Y. Wang, C. Moreau, R.S. Lima, J. Mesquita-Guimarães, E. Garcia, P. Miranzo, and M.I. Osendi

(Submitted May 22, 2010; in revised form September 17, 2010)

Yttria-stabilized zirconia (YSZ)-mullite multilayer architectures with compositional grading between the bond coat and YSZ top coat are envisioned as solutions to ease their coefficient of thermal expansion mismatch induced stress. In this work, two different types of mullite powder (spray-dried and freeze-granulated) and a mullite-YSZ 75/25 vol.% mixture spray-dried powder were employed. Using instrumented indentation with loads between 10 and 500 mN, the role of the powder characteristics on the mechanical behavior of air plasma-sprayed mullite bond coats deposited on SiC substrates was investigated. Hardness (*H*) and elastic modulus (*E*) were measured for the as-sprayed coatings and for coatings heat-treated at 1300 °C, in water vapor environment, for periods up to 500 h. Both *H* and *E* values of the coatings are found to be highly dependent on the size distribution of the starting powders. It is aimed the fabrication of an efficient and cost-effective EBC prototype based on YSZ compositionally graded mullite.

Keywords elastic modulus, environmental barrier coatings, heat-treatment, mullite, water vapor, YSZ

1. Introduction

In the quest to replace metallic components, for instance in specific hot-sections of gas turbine engines, multilayered environmental barrier coatings (EBCs) are envisioned and tested to protect Si-based ceramics (e.g., SiC and Si_3N_4) (Ref 1-3). Mullite ($3Al_2O_3{\cdot}2SiO_2$) is a low cost refractory oxide that currently constitutes the building block of an efficient EBC architecture. Mullite has a low thermal expansion coefficient (4.5-5.6 $\times$ 10^{-6}/°C) that represents, for instance, a close match with SiC (4.02 $\times$ 10^{-6}/°C) and excellent high temperature properties (e.g., high thermal shock and thermal stress resistance) offered mainly by its interlocking grain structure (Ref 4). In addition to the above-mentioned high-temperature properties, a second essential requirement of an EBC system is its stability in high temperature environments containing water vapors. A low permeability for oxidant species, good chemical compatibility with the Si-based substrate and silica scale formed from oxidation are mandatory features for an EBC so as to inhibit its major degradation mechanism namely the formation of volatile silicon hydroxide ($Si(OH)_4(g)$) when subjected to a corrosive water vapor containing environment originated from the combustion of the fuel (e.g., kerosene). Therefore, a suitable protective coating for gas turbine engine components formed of Si-containing materials essentially must fulfill a dual role serving as a thermal barrier and simultaneously providing environmental protection (Ref 5).

Mullite alone does not meet both requirements since it does not possess a good resistance to H_2O vapor attack (Ref 6) and a way to overcome this shortcoming is the use of layered coatings that as an ensemble offers the sought functionality. Consequently, functionally graded materials (FGMs), with discrete or continuous variations in composition and structure, showing corresponding changes in their properties have been introduced to applications where a certain functional requirement of a component is position dependent (Ref 7, 8). Mullite-based multilayer architectures, for instance, with compositional grading between the mullite bond coat and a yttria-stabilized zirconia (YSZ) top coat (showing excellent resistance to H_2O vapors attack) might offer a solution to ease their coefficient of thermal expansion (CTE) mismatch induced stress (Ref 9). To estimate the CTE values of composites several theoretical models such as the rule of mixture (ROM) or Turner model can be applied (Ref 10). In this

This article is an invited paper selected from presentations at the 2010 International Thermal Spray Conference and has been expanded from the original presentation. It is simultaneously published in *Thermal Spray: Global Solutions for Future Applications, Proceedings of the 2010 International Thermal Spray Conference*, Singapore, May 3-5, 2010, Basil R. Marple, Arvind Agarwal, Margaret M. Hyland, Yuk-Chiu Lau, Chang-Jiu Li, Rogerio S. Lima, and Ghislain Montavon, Ed., ASM International, Materials Park, OH, 2011.

C.V. Cojocaru, Y. Wang, C. Moreau, and **R.S. Lima**, National Research Council of Canada (NRC), Industrial Materials Institute (IMI), Boucherville, QC, Canada; and **J. Mesquita-Guimarães, E. Garcia, P. Miranzo,** and **M.I. Osendi**, National Research Council of Spain (CSIC), Institute of Ceramics and Glass (ICV), Madrid, Spain. Contact e-mail: cristian.cojocaru@cnrc-nrc.gc.ca.

context, the CTEs of the mullite-YSZ composites vary according to their respective volume fractions. For instance, using data taken from the existing literature for the thermal expansion coefficients, bulk modulus of both mullite and YSZ (Ref 4, 11) and applying the models mentioned above values of 6-7 $\times$ 10^{-6}/°C for a mullite/YSZ 75/25 vol.% and of 7.5-8.3 $\times$ 10^{-6}/°C for a mullite/YSZ 50/50 vol.%, respectively, are obtained. This gradual transition toward the CTE value of YSZ (10.6 $\times$ 10^{-6}/°C) is pictured as a potential solution to ease the stress induced by the bond and top coats CTE mismatch. A proper understanding of the mechanical properties such as the elastic modulus, hardness or plastic/elastic recovery work serves for an efficient design of such refractory oxide multilayers.

In this work, two different types of mullite powder (i.e., spray-dried and freeze-granulated) and a mullite-YSZ 75/25 vol.% mixture powder were employed. Using depth-sensing indentation with loads in the range 100-500 mN, the mechanical behavior of air plasma-sprayed mullite bond coats deposited on SiC substrates was assessed. Fully crystalline as-sprayed mullite coatings were engineered under controlled deposition conditions. Their mechanical properties were measured for the as-sprayed coatings as well as for coatings heat-treated at 1300 °C, in H_2O vapor environment, for periods up to 500 h. It was aimed the fabrication of an efficient and cost-effective EBC prototype based on YSZ compositionally graded mullite.

2. Experimental

2.1 Sample Preparation

Two types of mullite powders with different size distribution were employed in these studies: (i) spray-dried (d_{50} = 5 μm), further referred as M_SD and (ii) freeze-granulated (d_{50} = 55 μm), further referred as M_FG, both from the Institute of Ceramics and Glass (ICV)—CSIC, Madrid, Spain (Ref 12). Scanning electron microscope (SEM) images and particle size distribution of the mullite powders used are shown in Fig. 1(a) and (b). The particle size distributions were measured using a laser scattering particle size analyser (LS 13320, Beckman Coulter, Miami, FL). The morphology and size distribution of a mixed mullite-YSZ powder (75/25 vol.%) from ICV-CSIC, Madrid, Spain is also shown in Fig. 1(c). This mixture was produced using mullite and 7 wt.% Y_2O_3-stabilized zirconia (TZ4Y, Tosoh, Tokyo, Japan) powders. YSZ powder is 99.95% pure and with an average particle size of 0.3 μm. It is important to highlight that both M_SD, M_FG, and mullite-YSZ particles exhibit a similar porous-type structure.

The powders were sprayed onto sintered α-SiC (Hexoloy SA, Saint-Gobain, Worchester, MA) 5 $\times$ 5 cm substrates, via an axial atmospheric plasma spray (APS) torch (Axial III, Northwest Mettech, North Vancouver, BC, Canada). The Axial III plasma spray torch is a three anode-three cathode plasma torch with axial injection feed of the powder. Fully crystalline as-deposited coatings were

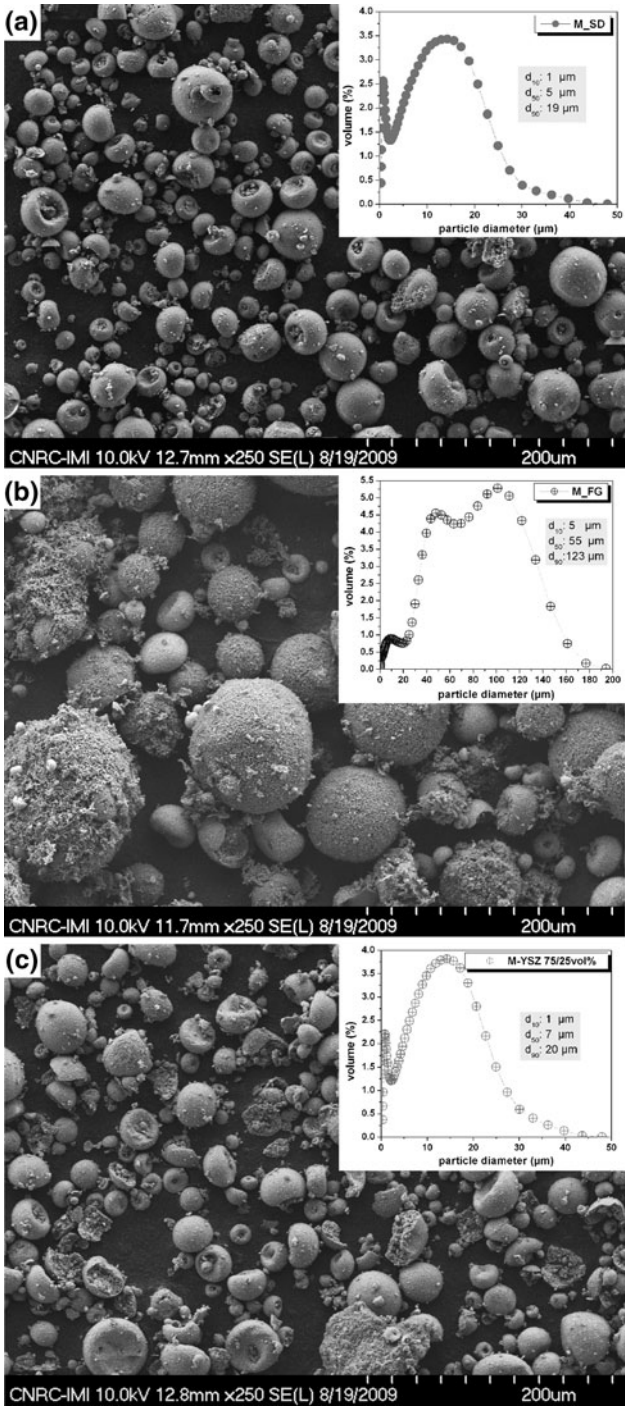

Fig. 1 SEM micrographs of the mullite M_SD, M_FG, and M-YSZ 75/25 vol.% mixture powders used throughout the experiments. Their corresponding size distributions are shown in the insets

engineered in all cases by properly controlling the plasma spray parameters and substrate temperature during spraying (proprietary NRC technology). Combinations of mullite/YSZ powders (ICV-CSIC, Madrid, Spain) such as mullite-YSZ 75/25 vol.% have been further deposited on top of the mullite bond coats so as to produce bi and

tri-layer coatings with an YSZ compositional grading. After completing the spraying process the 5 × 5 cm coupons were cut in quarters for structural/mechanical analysis and thermal treatment (TT).

2.2 Structural Characterization and Thermal Treatment

A diffractometer (D8-Discovery, Brucker AXS Inc. Madison, WI) using Cu K_α radiation in Bragg-Brentano (θ-2θ) configuration was used to analyze the phase composition of both as-sprayed and thermally treated coatings. The diffracted signal was collected over a 2θ range of 20°-60° with a step size of 0.02° and a 5 s/step acquisition time through a 1° fine collimator slit.

After x-ray diffraction (XRD) characterization, samples were embedded in epoxy prior to cross-section cutting and further prepared by standard metallographic procedures for field-emission scanning electron microscopy (FE-SEM) (S4700, Hitachi Ltd., Tokyo, Japan). Porosity of each mullite coating forming the bi-layer structures was determined using image analysis (IA) of SEM micrographs. Three (3) samples were analyzed per coating and a number of eight cross-section SEM images per coating (encompassing the entire width of the coating) were captured and binarized. Porosity was measured as area percentage of dark features (pores) with image analysis software from Leica.

TT tests were performed at 1300 °C and 1 atm, in a H_2O vapor environment (90% H_2O/10% air and continuous flow of ~3.5 cm/s) for time intervals up to 500 h using an in-house developed EBC test rig and based on a high-temperature tube furnace (STT-1700-2.0-18, SentroTech, Berea, OH).

2.3 Mechanical Testing via Instrumented Indentation Testing

Instrumented indentation testing (IIT) was performed using a Nanoindenter G200 (Agilent Technologies, Oak Ridge, TN). Hardness (H) and elastic modulus (E) of each deposited coating were measured at room temperature on the polished cross section of the sample, via Oliver-Pharr method (depth-sensing indentation) (Ref 13) making use of a Berkovich diamond tip. The applied indentation loads and the corresponding penetration depths (tip displacements into surface) were measured continuously during each loading-unloading cycle. Thus, the main advantage of using depth-sensing indentation consists in the fact that the residual indentation impression does not have to be directly imaged as in conventional indentation testing. The elastic (Young's) modulus of the coating material was determined, using the stiffness calculated from the slope of the load-displacement curve at the maximum load, during each unloading cycle. This serves to initially determine the reduced elastic modulus (E_r) which is further used to determine E value of the test material (Ref 13). The indenter diamond tip properties used for calculations were $E_i = 1141$ GPa and Poisson's ratio $\nu_i = 0.07$ and a numerical factor $\beta = 1$ for the triangular cross sections of the Berkovich tip. The Poisson's ratio of the tested coatings was assumed to be 0.25, which is a typical value used for ceramic materials. This inference ($\nu = 0.25 \pm 0.1$) produces only about a 5% uncertainty in the calculated value of E for most materials.

The measurements were performed at loads between 100 and 500 mN with loading times of 15 s and unloading (90% record of the segment) of 20 s. For each sample, sets of 15-20 indents were performed (either in form of arrays or on selected locations) with distances between indents in the range of 25-50 μm and correlated with the applied load. Example of such indentations carried out in the form of an array onto a coating cross section is shown in Fig. 2.

3. Results and Discussion

3.1 Microstructural Analysis

XRD patterns revealed fully crystalline as-sprayed coatings in both cases as shown in Fig. 3(a). The intrinsic nature and difference in the size distribution between the M_SD (spray-dried) and M_FG (freeze-granulated) mullite powders may explain the formation of a secondary γ-Al_2O_3 phase initially observed within the M_SD as-sprayed coatings. More specifically, the small M_SD particles (Fig. 1a) may have lost part of their silica content (via volatilization) due to the high temperatures of the plasma jet, resulting in the formation of molten alumina-rich particles during spraying. These molten alumina-rich particles would tend to re-solidify into the γ phase of alumina during spraying, as described by McPherson (Ref 14). This event would tend to be less pronounced with the FG powder (Fig. 1b) due to the larger particle sizes and masses.

However, thermally treated coatings up to 500 h at 1300 °C in H_2O vapor environment for both M_SD and

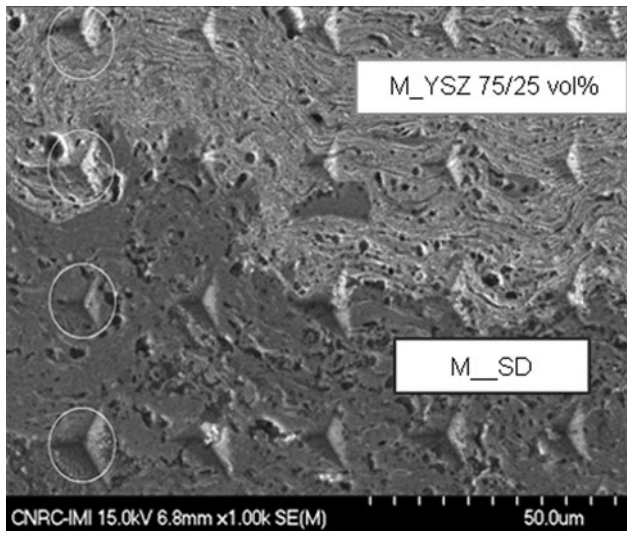

Fig. 2 Indentation testing residual impression arrays made into a M_SD/M-YSZ 75/25 vol.% bi-layer with a Berkovich diamond tip

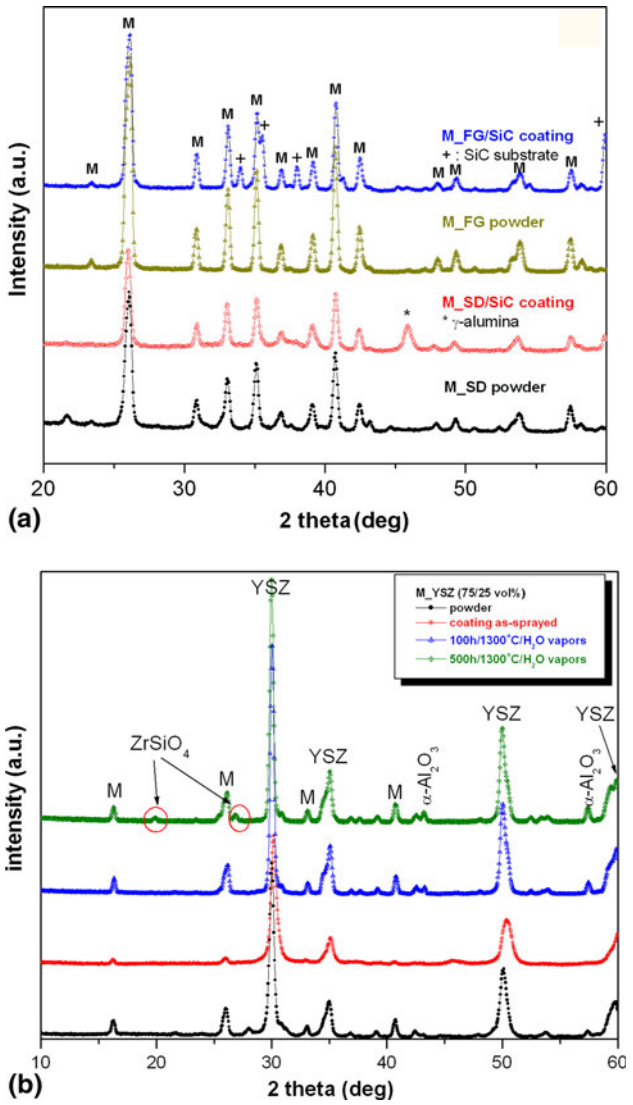

Fig. 3 (a) XRD patterns of powders and as-sprayed corresponding coatings and (b) phase evolution of M-YSZ 75/25 vol.% top-coat with thermal treatment at 1300 °C, in H_2O vapors, up to 500 h time intervals

M_FG do not show any foreign phases and exhibit a high degree of crystallinity. In the case of bi-layer structures with a M-YSZ (75/25 vol.%) top coat main peaks of tetragonal YSZ and mullite are detected and also small peaks of α-Al_2O_3. One notable aspect is the detection of $ZrSiO_4$ (zircon) peaks in the samples thermally treated up to 500 h as indicated in Fig. 3(b), reaction that may have occurred when $Si(OH)_4$ gaseous species bind to the ZrO_2 sites. A reaction between the mullite and YSZ phases of the powder at high temperature exposure could also be the origin of the zircon formation. A more extensive structural and phases composition characterization of the coatings is given in Ref 15.

Typical as-sprayed bi-layer coating architectures are shown in Fig. 4 (a) and (b). SEM analyses reveal dense coatings with good adhesion between both substrate and layers, however, periodically spaced vertical cracks were detected in both cases. The M_SD-powder-based coatings (Fig. 4c) appear to be denser, whereas, the M_FG-powder-based ones exhibit a higher amount of semi-molten (freeze-granulated) particles indicated by arrows in Fig. 4(d), where bi-layer interfaces details are illustrated. The microstructural differences of these types of mullite bond coats are highly linked to the differences of particle size distribution. The difference in thickness between M_SD and M_FG coatings arises from the different degree of melting of the particle and different deposition efficiencies. Both coatings were sprayed using the same set of spray conditions and number of torch passes across the substrate. Therefore, as the M_SD powder particles (Fig. 1a) are smaller than those of the M_FG (Fig. 1b), the M_SD coatings will tend to be denser as the extent of melting of in-flight particles is likely higher in this case. Indeed, the porosity measurements performed via IA of SEM micrographs indicate values of 9% for the M_SD coatings, whereas higher values of 30% are recorded for the as-sprayed M_FG coatings.

Investigation of the SiC-mullite bond coat interfaces after TTs shows how the vertical cracks (and porosity for the M_FG coating) represented favorable paths for the oxidizing species to reach the substrate. Formation of a ~2-μm-thick silica interface layer between SiC and M_SD and of a ~6-μm-thick silica interface layer between SiC and M_FG are measured after 500 h TT at 1300 °C in the presence of water vapors (Fig. 5a, b). On the other hand, these cracks (and the porosity of the M_FG coating) may offer the essential stress compliance when the parts are subjected to thermal cycling functioning. Future testing under thermal cycling will have to be done to better evaluate the tradeoff between these coating features and silica growth.

3.2 Mechanical Characterization and Indentation Load Effect

Thermally sprayed coatings are in general well suited to mechanical assessment by instrumented indentation. The capability to select the location of the indentation enables testing the coating within its thickness avoiding areas with high level of porosity that in some cases might lead to erroneous values. The load on the sample is defined as the force with which the indenter tip is impinging on the surface and depth is measured from the contact point of the tip with the sample. The influence of indentation load on hardness and Young's modulus of ceramics has been investigated by several groups (Ref 16). It was reported that both H and E exhibit significant dependence on the indentation load which in the case of brittle materials such as ceramics has been attributed to a surface "sinking-in" phenomenon. A general trend is that hardness and elastic moduli tend to decrease with the increase of the applied load (Ref 17). To verify these assumptions, measurements were performed on the deposited coatings by varying the indentation loads from 10 to 500 mN and searching for the interval values of the applied force for which the obtained

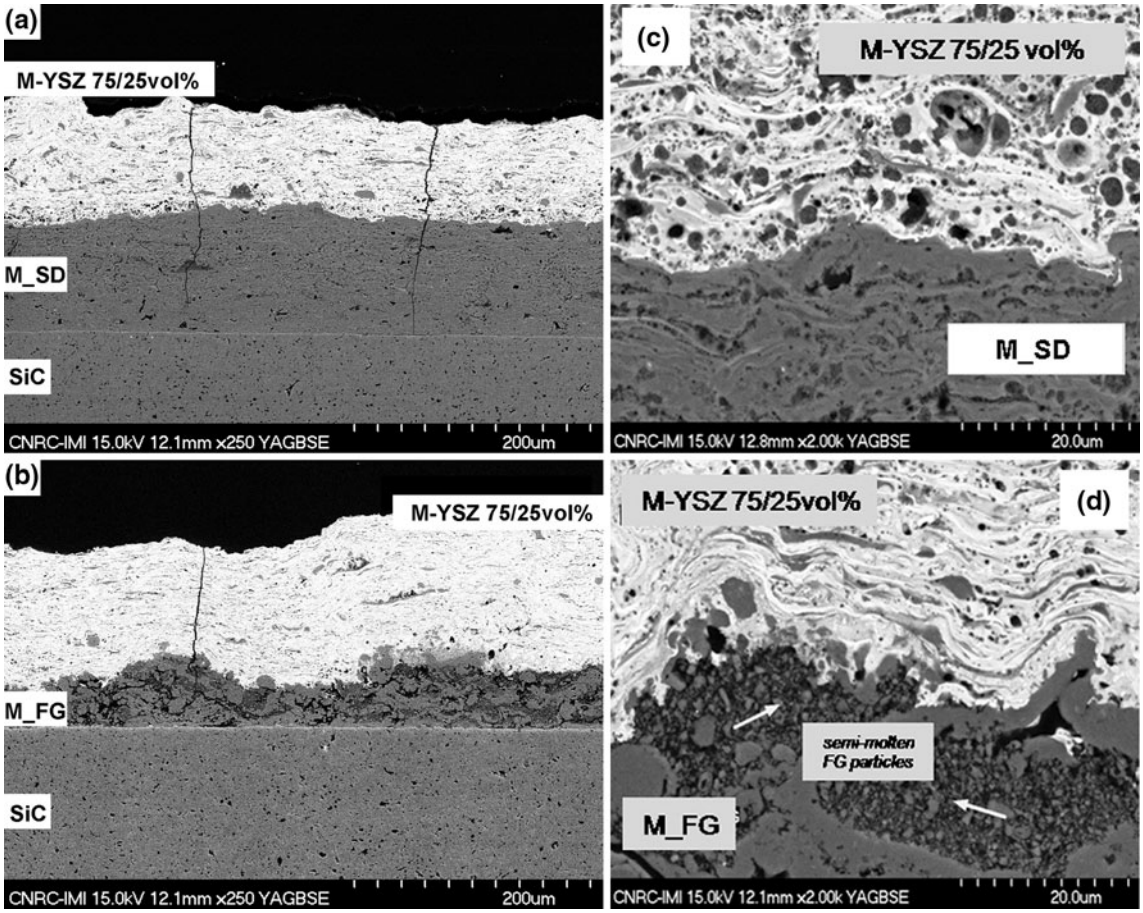

Fig. 4 (a) SEM image of the as-sprayed mullite M_SD/M-YSZ 75/25 vol.% bi-layers and (b) SEM image of the as-sprayed mullite M_FG/M-YSZ 75/25 vol.% bi-layers, (c) SEM detail of the as-sprayed M_SD/M-YSZ 75/25 vol.% bi-layer interface, and (d) SEM detail of the as-sprayed mullite M_FG/M-YSZ 75/25 vol.% bi-layer interface showing very good adhesion

H and *E* data stabilized. A more detailed analysis on the indentation size effects on *E* values of mullite-BSAS plasma-sprayed coatings is presented in Ref 18. It was observed that within the load interval 250-500 mN, both *H* and *E* values start to stabilize and at this point it is hypothesized that the measured values represent a global perspective on the material and not only probing small volumes of its microstructure. The size of the indentation impression at loads of 500 mN (50 gf) is about ~15 μm (see Fig. 2). Typical APS ceramic splats exhibit thicknesses in the order of 1 μm. Therefore, when areas representing triangular impression sizes of ~15 μm are probed (i.e., probed volumes ~80 μm^3) a group of many splats together with the inherent porosity between the splats is tested and not just one single or few splats. This offers a more than local perspective of the coating's elastic modulus and the porosity is taken into account. Based on these experimental observations, the indentation load of 500 mN was chosen to probe the coatings of this work and measure the respective mechanical properties. It was assumed that the *E* and *H* values measured at 500 mN would tend to represent the overall behavior of the coatings.

3.3 Analysis of Load-Displacement Curves

The load-depth curves recorded for mullite layers (i.e., M_SD and M_FG) and the M-YSZ-mixture-based layer, reveal different slopes during unloading which implicitly mean different Young's moduli. It is observed that in some cases, the penetration depth (displacement) within the M_FG coatings is much deeper (3.5 μm) compared to the M_SD coatings (2 μm) instantly suggesting lower hardness values of the former. Also the spread range of the penetration depths values indicate a larger overall microstructural non-homogeneity of the M_FG coatings, which can be related to the broader size distribution of the powder and their incomplete melting during the spraying process. These experimental results are in agreement with the results expected based on the microstructural characteristics of the M_SD (Fig. 4a, c) and M_FG (Fig. 4b, d) coatings and the porosity values obtained for the as-sprayed coatings.

Mean values (15 indentations) obtained for hardness and elastic modulus for layered coating architectures both the as-sprayed state and thermally treated (up to 500 h) are provided in Table 1. For an even more complete

interpretation of the obtained values, the hardness and elastic modulus values of M_SD and M_FG powder-based coatings were also compared with the values of fully crystalline as-sprayed mullite coatings obtained with a commercially available powder, i.e., fused and crushed (further referred as M_SG), $d_{50} = 50$ μm (Saint Gobain #1020, Saint-Gobain, Worchester, MA) used in the above-mentioned study (Ref 18).

Both H and E values measured for the coatings deposited with the custom prepared M_SD are higher than those of the coatings obtained with the M_FG powder. This result is in concordance with both the porosities and microstructures of the respective coatings that are dictated primarily by the particle size distribution of the powders. The larger size distribution of the M_FG mullite powders will tend to generate higher porosity levels (~30% porosity estimated via IA) since in this case the power of the torch was not high enough so as to melt completely the majority of the powder particles. Therefore, as shown in Fig. 5(b), the M_FG-based coatings exhibit also a higher level of un-molten particles. These combined effects lead to a decrease in the M_FG hardness and elastic modulus values. Furthermore, the values presented in Table 1 suggest a better match between the E and H values of the M_SD-based bond coat and M-YSZ 75/25-based layer than those between the M_FG and M-YSZ 75/25 coatings. Although both M-YSZ 75/25 coatings were deposited under the same conditions, the underlying ''substrate'' material for these coatings is different (M_SD in one case and M_FG in the other), which is likely to cause a difference in the residual stress levels and the elastic properties of the coatings. In this respect, the different stress distributions in the top coats may explain the differences in the E and H values of M-YSZ 75/25 coatings shown in Table 1. It is hypothesized that a desirable layered architecture will be the one that demonstrates the lowest percentage of variation of E and H values, to reduce the strain levels in between layers. Also, when the E and H values of the M_SG coatings are compared to those of the M-YSZ 75/25 coatings, they exhibit smaller mismatch than M_FG/M-YSZ 75/25 coatings. Despite the fact that the both M_SD and M_SG powders exhibit different morphologies, the spraying of the dense individual fused and crushed M_SG particles will tend to produce relatively dense coatings (Ref 18) even if semi-molten particles are embedded in the coating microstructure. Therefore, it is not a surprise that the M_SD and M_SG mullite coatings tend to exhibit similar mechanical behavior, and both seem to be better candidates as bond coats for this type of architecture when using the M-YSZ 75/25 coating as transitional layer.

The effect of the TT on the hardness and the elastic modulus of the deposited coatings was also investigated. It was experimentally determined that H and E values for the mullite coatings produced from the fused and crushed M_SG and spray-dried M_SD powders increase with the duration of the heat treatment and follow the typical behavior expected for ceramic materials, which is caused by sintering effects (see Table 1). A different situation is

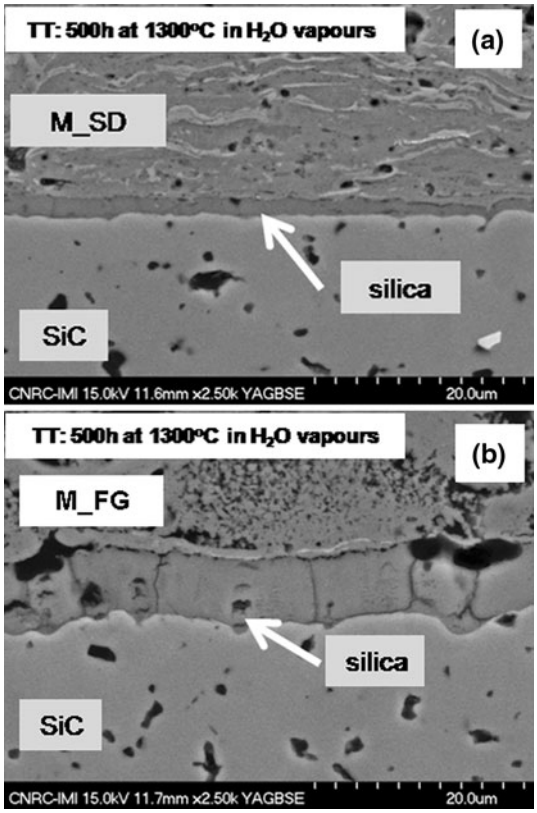

Fig. 5 SEM details of (a) SiC/M_SD and (b) SiC/M_FG interfaces showing silica scale formation after 500 h thermal treatment at 1300 °C in H_2O vapors

Table 1 ***E*** **and** ***H*** **values of the as-sprayed and heat-treated coatings for time intervals up to 500 h (bold rows represent bi-layer systems)**

	***E*, GPa**			***H*, GPa**		
EBC type/coating	**As dep.**	**100 h TT**	**500 h TT**	**As dep.**	**100 h TT**	**500 h TT**
EBC type I						
M_SD	**118 ± 17**	**155 ± 16**	**172 ± 16**	**6.1 ± 2**	**9.5 ± 2**	**10 ± 2**
M75/YSZ 25 vol.%	**127 ± 29**	**139 ± 16**	**168 ± 17**	**7.8 ± 3**	**8.4 ± 2**	**9.2 ± 1**
EBC type II						
M_FG	**90 ± 19**	**70 ± 8**	**69 ± 11**	**4.7 ± 2**	**2.6 ± 1**	**2.9 ± 1**
M75/YSZ 25 vol.%	**156 ± 13**	**162 ± 7**	**157 ± 16**	**11.9 ± 2**	**12.2 ± 2**	**11.8 ± 2**
M_SG	126 ± 16	174 ± 16	177 ± 17	7.8 ± 1.7	10 ± 1	12 ± 2

encountered in the M_FG-based coatings where the measurements do not denote a clear trend in the *H* and *E* values and basically any significant increase (variation) with annealing time. In this case, the TT tests in fact did not change the porosity of the M_FG samples annealed up to 500 h interval time (i.e., porosity values remain in the order of 30% for thermally treated coatings) and this correlates to the fairly steady trend for *E* and *H* values. On a first occurrence, the result is rather unexpected and up to this moment there are no strong evidences to explain these events.

When the overall as-sprayed and thermally treated microstructures of the mullite M_FG coating are compared via SEM (not shown here), there are no signs of densification related to sintering. The M_FG coating is highly porous, exhibiting a series of porous semi-molten agglomerated particles embedded in the coating microstructure (Fig. 4d, 5b). Concerning this specific issue, in a previous work (Ref 19), it was shown that nanostructured YSZ coatings produced via APS, exhibiting porous semi-molten agglomerated particles embedded in the coating microstructure (ceramic matrix), tend to exhibit a high resistance to sintering at high temperatures (1400 °C), which impeded a major increase of *E* values when compared to those of conventional YSZ APS coatings. Briefly, the sintering resistance is given by the shrinkage of these porous semi-molten embedded particles in the ceramic matrix at high temperature, which produces void formation within the overall coating microstructure. It has to be highlighted that the microstructures of these coatings are similar to those of the M_FG coatings. Consequently, it is hypothesized that a similar type of event may have occurred with the M_FG coatings and the void creation explains the larger penetration depths of the indenter after 100 and 500 h of heat exposure and its respective effect on the *E* and *H* values. Therefore, due to the high porosity levels (30% porosity) and the presence of semi-molten agglomerated particles embedded in the microstructure of the M_FG coatings, it is assumed that the heat-treatment performed at 1300 °C did not provide the necessary for overall coating densification. Further experimental investigations are underway to better understand and monitor if this unexpected behavior is present in architectures having a silicon (Si) bond-coat between the substrate and the FGM coatings.

4. Conclusions

Fully crystalline mullite and YSZ-compositionally graded mullite coatings have been produced via thermal APS under controlled deposition conditions. The elastic modulus and hardness of the coatings have been investigated via IIT and an analysis of the values obtained for a 500 mN indentation load has been pursued. It was found via systematic measurements that both *E* and *H* values of the as-sprayed coatings are highly dependent on the particle size distribution of the starting powders. As expected, a TT generally induced an increase of *E* and *H* values of the coatings produced from spray-dried and fused and crushed powders. However, the coating produced from the freeze granulated powder did not follow this trend. It is hypothesized that the high porosity levels of the coating create a strong barrier against sintering and densification effects.

It was identified a better match between the *E* and *H* values of the bond coat and subsequent layers obtained from powders having similar type and size distribution (e.g., M_SD/M-YSZ 75/25 vol.%). However, mechanical properties of coatings produced from particles with different morphologies (e.g., spray-dried and fused and crushed) can be matched and tailored if the deposition conditions are carefully controlled to produce coatings with similar microstructural features. Work is in progress to assess the *E* and *H* match in mullite-YSZ compositionally graded multilayers toward achieving architectures having a 100% YSZ top coat.

Acknowledgments

The NRC team of authors acknowledges valuable technical support from the technical officers of the Surface Technology Group for samples production, metallographic preparation, and SEM analysis. This work has been supported by NRC-CSIC program (project 2007CA003).

References

1. K.N. Lee, Current Status of Environmental Barrier Coatings for Si-Based Ceramics, *Surf. Coat. Technol.*, 2000, **133-134**, p 1-7
2. S. Latzel, R. Vaßen, and D. Stöver, New Environmental Barrier Coating System on Carbon-Fiber Reinforced Silicon Carbide Composites, *J. Therm. Spray Technol.*, 2005, **14**, p 268-272
3. K.N. Lee, D.S. Fox, and N.P. Bansal, Rare Earth Silicate Environmental Barrier Coatings for SiC/SiC Composites and Si_3N_4 Ceramics, *J. Eur. Ceram. Soc.*, 2005, **25**, p 1705-1715
4. H. Schneider, J. Schreuer, and B. Hildmann, Structure and Properties of Mullite: A Review, *J. Eur. Ceram. Soc.*, 2008, **28**, p 329-344
5. N.S. Jacobson, Corrosion of Silicon-Based Ceramics in Combustion Environments, *J. Am. Ceram. Soc.*, 1993, **76**, p 3-28
6. N.S. Jacobson, D.S. Fox, J.S. Smialek, E.J. Opila, C. Dellacorte, and K.N. Lee, Performance of Ceramics in Severe Environments, *ASM Handbook, Vol. 13B Corrosion Materials*, p 565
7. U. Schulz, M. Peters, Fr.-W. Bachb, and G. Tegeder, Graded Coatings for Thermal, Wear and Corrosion Barriers, *Mater. Sci. Eng. A*, 2003, **362**, p 61-80
8. T.W. Murray, O. Balogun, T.L. Steen, S.N. Basu, and V.K. Sarin, Inspection of Compositionally Graded Mullite Coatings Using Laser Based Ultrasonics, *Int. J. Refract. Met. Hard Mater.*, 2005, **23**, p 322-329
9. C. Cano, E. Garcia, A.L. Fernandes, M.I. Osendi, and P. Miranzo, Mullite/ZrO_2 Coatings Produced by Flame Spraying, *J. Eur. Ceram. Soc.*, 2008, **28**, p 2191-2197
10. P.K. Rohatgi, N. Gupta, and S. Alaraj, Thermal Expansion of Aluminum-Fly Ash Cenosphere Composites Synthesized by Pressure Infiltration Technique, *J. Compos. Mater.*, 2006, **40**(13), p 1163-1174
11. R. Asthana, A. Kumar, and N.B. Dahotre, *Materials Processing and Manufacturing Science*, Elsevier, Amsterdam, 2006
12. E. Garcia, J. Mesquita-Guimarães, P. Miranzo, and M.I. Osendi, Procedure for Obtaining Ceramic Feedstock for Thermal

Spraying Applications, Patent 2009, ICV-CSIC, Ref. ES1641.581, Spain
13. W.C. Oliver and G.M. Pharr, Measurement of Hardness and Elastic Modulus by Instrumented Indentation: Advances in Understanding and Refinements to Methodology, *J. Mater. Res.*, 2004, **19**(1), p 3-20
14. R. McPherson, A Review of Microstructure and Properties of Plasma sprayed Ceramic Coatings, *Surf. Coat. Technol.*, 1989, **39-40**, p 173-181
15. E. Garcia, J. Mesquita-Guimarães, P. Miranzo, M.I. Osendi, C.V. Cojocaru, Y. Wang, C. Moreau, and R.S. Lima, Phase Composition and Microstructural Responses of Crystalline Mullite/YSZ Coating Under Water Vapor Environments, *Thermal Spray: Global Solution for Future Application (ITSC 2010 Proceedings)*, DVS-Verlag GmbH, Dusseldorf, Germany, 2010, PDF Format (CD)
16. A.A. Elmustafaa and D.S. Stone, Nanoindentation and the Indentation Size Effect: Kinetics of Deformation and Strain Gradient Plasticity, *J. Mech. Phys. Solids*, 2003, **51**, p 357-381
17. B.-K. Jang, Influence of Low Indentation Load on Young's Modulus and Hardness of 4 mol% Y_2O_3-ZrO_2 by Nanoindentation, *J. Alloy Compd.*, 2006, **426**, p 312-315
18. C.V. Cojocaru, S. Kruger, C. Moreau, and R.S. Lima, Mechanical Properties and Behaviour of BSAS/Mullite-Based Environmental Barrier Coatings Exposed to High Temperature in Water Vapour Environment, *Thermal Spray: Global Solution for Future Application (ITSC 2010 Proceedings)*, DVS-Verlag GmbH, Dusseldorf, Germany, 2010, PDF Format (CD)
19. R.S. Lima and B.R. Marple, Toward Highly Sintering-Resistant Nanostructured ZrO_2-7 wt.% Y_2O_3 Coatings for TBC Applications by Employing Differential Sintering, *J. Therm. Spray Technol.*, 2008, **17**, p 846-852